

## Oscillating instability in bouncing droplet crystals

This article has been downloaded from IOPscience. Please scroll down to see the full text article.

2011 EPL 94 20004

(<http://iopscience.iop.org/0295-5075/94/2/20004>)

View [the table of contents for this issue](#), or go to the [journal homepage](#) for more

Download details:

IP Address: 130.89.74.179

The article was downloaded on 11/01/2012 at 14:43

Please note that [terms and conditions apply](#).

# Oscillating instability in bouncing droplet crystals

A. EDDI<sup>1(a)</sup>, A. BOUDAUD<sup>2</sup> and Y. COUDER<sup>1</sup>

<sup>1</sup> *Matières et Systèmes Complexes, Université Paris 7 Denis Diderot, CNRS - UMR 7057 - Bâtiment Condorcet, 10 rue Alice Domon et Léonie Duquet, 75205 Paris cedex 13, France, EU*

<sup>2</sup> *Laboratoire de Reproduction et Développement des Plantes, INRA, CNRS, ENS, Université de Lyon, UMR 5667 46 allée d'Italie, 69364 Lyon Cedex 07, France, EU*

received 13 January 2011; accepted in final form 15 March 2011

published online 15 April 2011

PACS 05.45.-a – Nonlinear dynamics and chaos

PACS 47.55.D- – Drops and bubbles

PACS 63.22.-m – Phonons or vibrational states in low-dimensional structures and nanoscale materials

**Abstract** – Bouncing droplets on a vibrated liquid bath can interact via the surface waves they emit and form various types of stable crystalline clusters. When increasing the forcing acceleration over an onset value, the aggregates present a global and spontaneous vibration mode. Here, we investigated experimentally these vibrations in hexagonal and square lattice clusters and show that there is a long-range selection amongst the modes. We propose a physical interpretation of the instability based on the intrinsic delay due to wave propagation and a simple model that explains the observed features of the vibrations.

Copyright © EPLA, 2011

**Introduction.** – Droplets can bounce on a vertically vibrated liquid surface [1]. Their bouncing emits damped surface waves that mediates an interaction between them. If the surface on which it bounces is slanted, a given droplet receives a non-vertical kick and thus moves in the horizontal plane [2]. It can find an equilibrium position only if it bounces in a location where the average slope during the contact is zero. The corresponding wave-mediated interaction allows not only the creation of self-propelling droplet associations [3], but also the stabilization of regular macroscopic aggregates of droplets [2,4,5]. In these stable arrangements, each droplet settles in the trough formed by the first antinode of the wave generated by its nearest neighbours. It was shown that the bouncing can become sub-harmonic. In this case, the waves emitted are almost sustained because of the proximity to the Faraday instability [6,7]. As the droplets can have two different phases and have a long-range periodic interaction, it allows the formation of complex patterns, including squares, hexagons and octagons [8]. These structures are stable on the bath for several hours.

Inside the aggregate, the droplets are massive interacting objects evolving in a potential trap given by the wave-mediated interaction. They thus form an original periodic mass-spring chain. Here, we investigate

a spontaneous instability of this periodic pattern when the forcing acceleration, used as the control parameter, is increased.

**Experimental set-up.** – We use a silicone oil bath (density  $\rho = 965 \text{ kg} \cdot \text{m}^{-3}$ , surface tension  $\sigma = 20.9 \cdot 10^{-3} \text{ N} \cdot \text{m}^{-1}$  and viscosity  $\mu = 50 \cdot 10^{-3} \text{ Pa} \cdot \text{s}$ ) with thickness  $h_0 = 6 \text{ mm}$ . It is subjected to a vertical harmonic acceleration  $\gamma = \gamma_m \cos(2\pi f_0 t)$  by a vibration exciter (Bruel & Kjaer 4808). The driving frequency is set to  $f_0 = 50 \text{ Hz}$ . We select the droplet diameter  $D = 900 \pm 20 \mu\text{m}$  by optical means. The forcing acceleration is large enough to ensure that the droplets bounce with the Faraday frequency  $f_F = f_0/2$  [2,8]. The wavelength  $\lambda_F = 2\pi/k_F = 6.95 \text{ mm}$  on the bath is given by inserting the bouncing pulsation  $\omega_F = 2\pi f_F$  in the dispersion relation for surface waves:

$$\omega^2 = [gk + (\sigma/\rho)k^3] \tanh(kh). \quad (1)$$

We also define the Faraday phase speed  $v_\varphi^F = \omega_F/k_F = 173 \text{ mm} \cdot \text{s}^{-1}$ . Similar results have been obtained with  $\mu = 20 \cdot 10^{-3} \text{ Pa} \cdot \text{s}$ ,  $f_0 = 80 \text{ Hz}$ ,  $\lambda_F = 4.75 \text{ mm}$ ,  $v_\varphi^F = 190 \text{ mm} \cdot \text{s}^{-1}$  and  $D = .8 \text{ mm}$ .

We build macroscopic clusters with hexagonal or square symmetry by gathering droplets following the building rules described elsewhere [8]. Hexagonal aggregates (see fig. 1(a) and movie1\_1.mov) bind with an equilibrium

<sup>(a)</sup>E-mail: antonin.eddi@univ-paris-diderot.fr

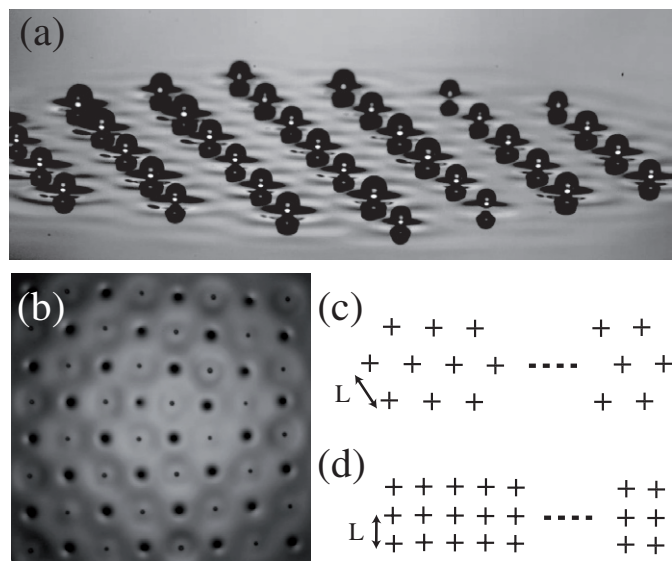


Fig. 1: (a) Side-view snapshot of a hexagonal lattice aggregate of bouncing droplets. (b) Top-view snapshot of 49-droplets square lattice aggregate. (c) and (d) Schematic view of line-shaped aggregates, standing for one-dimensional aggregates with (c) hexagonal lattice or (d) square lattice. In both cases,  $L$  is the lattice constant.

distance  $L = 11.5$  mm. For square aggregates, the binding distance is smaller, *i.e.*  $L = 8.1$  mm. We can choose at will the shape of the outer envelope of the cluster when gathering the droplets. Using image processing, we can follow the position of each droplet during the experiment with a spatial resolution of  $0.04$  mm. The movies are recorded at 10 images per second.

**Instability in one-dimensional aggregates.** – We create on the bath quasi-one-dimensional aggregates. In this case, there are  $N$  droplets ( $N > 10$ ) along one direction and only three droplets transversally (see fig. 1(c-d)). When slowly increasing the forcing acceleration  $\gamma_m$ , an onset value  $\gamma_V = 3.5 \pm 0.05 g$  is reached above which a spontaneous oscillation of the position of each droplet is observed. The transient regime (see fig. 2) to oscillation is obtained by setting  $\gamma_m$  to a value slightly larger than  $\gamma_V$  at  $t = 0$ . We observe the growth of a collective vibration along the aggregate. All the droplets move at the same frequency  $f_V$  with first neighbours oscillating with opposite phases. The oscillation mode saturates to a stationary amplitude of typically 10% of the distance between two droplets (see [movie2.mov](#)). Measurement of the vibration frequency  $f_V$  by FFT show very little variation with the length of the aggregate, giving  $f_V = 1.00 \pm 0.05$  Hz for hexagonal lattice aggregates. Note that  $f_V \ll f_F$ .

This instability corresponds to a spatial modulation of the periodic pattern. This mode is coherent all over the aggregate structure. As the second neighbours of a droplet have in-phase motions, the selected mode has a

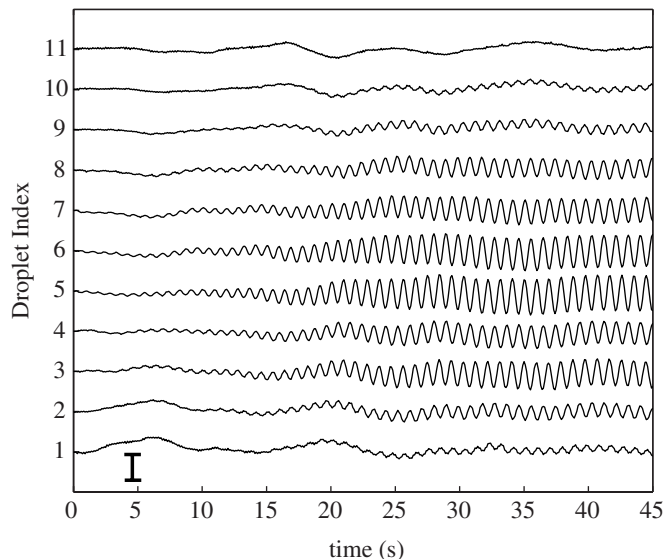


Fig. 2: Trajectories along a line of 11 droplets in hexagonal symmetry when the forcing acceleration  $\gamma_m$  is set to a value slightly larger than  $\gamma_V$  at  $t = 0$ . The black segment has a length equal to  $L/10$ . Each droplet is moving in phase opposition with its neighbours.

spatial wave number  $k_V = \pi L$ . This is the largest wave number possible in a vibrating structure, corresponding to an optical mode. Along a line of droplets, we can separate two populations into the aggregate, which can be labelled (+) and (-) if the droplets have in-phase or out-of-phase oscillations with a reference droplet. This creates two sublattices of droplets having the same vibrational properties. Each vibrating sub-network has a spatial periodicity which is twice the original network periodicity.

The growth of the oscillation mode occurs at the center of the aggregate and the stationary amplitude is weaker on the edges. If we decrease the forcing acceleration  $\gamma_m$ , all the droplets return to their former position. In contrast, when we further increase our control parameter, the oscillations of the central droplets become so large that one of them is able to leave its potential trap and collapses with one of its neighbours. The destruction of the aggregate always occurs from the center, contrary to the habitual melting process occurring at the edges.

The observed destabilization is a secondary instability of a non-linear periodic pattern. Theoretical studies have shown that spatially periodic systems present various types of instabilities towards dynamical states. Depending on the symmetry breaking involved, there are ten generic modes [9]. A large number of these solutions have been illustrated in various experiments such as Taylor-Couette flows [10], Rayleigh-Benard convection [11], or directional viscous fingering [12]. The theory predicts that the types of instabilities are related to the symmetry breaking involved. For example, drifting domains (attested experimentally in [13,14]) have been associated with the breaking of left-right symmetry. The solution that we

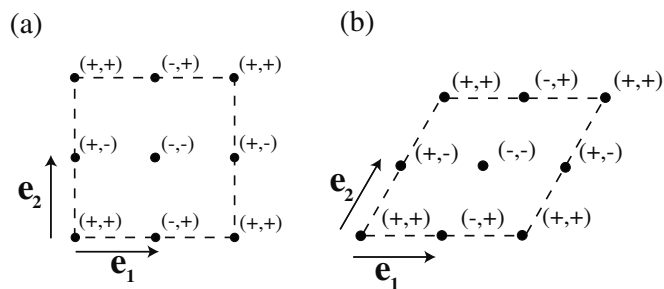


Fig. 3: Schematic representation of the four sub-populations  $(+,+)$ ,  $(+,-)$ ,  $(-,+)$  or  $(-,-)$  of droplets in (a) square geometry and (b) hexagonal geometry.

observe experimentally is reminiscent of temporal period doubling: the secondary instability has a wavelength which is twice the original wavelength. This kind of oscillatory modes has been observed in solidification [14], viscous fingering [12] or liquid columns [13,15].

**Two-dimensional aggregates.** – We build regular aggregates, with either square or hexagonal symmetry. The onset  $\gamma_V$  of vibration depends on the geometry of the aggregates, and is around  $\gamma_V = 3.5 \pm 0.05 g$  for hexagonal symmetry clusters. Using square lattice aggregates, we obtain a forcing threshold  $\gamma_V = 3.25 \pm 0.05 g$  and a vibration frequency  $f_V = 1.33 \pm 0.05$  Hz.

The two-dimensional aggregates have two principal directions, which can be represented by two vectors  $\mathbf{e}_1$  and  $\mathbf{e}_2$ , the angle between  $\mathbf{e}_1$  and  $\mathbf{e}_2$  is  $\pi/2$  in square aggregates and  $\pi/3$  in the hexagonal ones (see fig. 3). Choosing the norm of  $\mathbf{e}_1$  and  $\mathbf{e}_2$  equal to  $L$ , the periodicity of the network, a droplet of the lattice is located at  $m\mathbf{e}_1 + n\mathbf{e}_2$ , with  $(m, n) \in \mathbb{Z}^2$ . Using a classical description, we can define the unit cell in the lattice as a parallelogram with vertices in  $(0, 0)$ ,  $(\mathbf{e}_1, 0)$ ,  $(0, \mathbf{e}_2)$  and  $(\mathbf{e}_1, \mathbf{e}_2)$ . The unit cell is either a square with  $L$  side in the square aggregates, or a rhombus in the hexagonal aggregates.

When  $\gamma_m > \gamma_V$ , the same period doubling as in the one-dimensional case occurs along the principal directions of the lattice. The network will now be invariant under translations of  $2\mathbf{e}_1$  or  $2\mathbf{e}_2$ . The unit cell is four times larger than the original unit cell. Whatever the geometry, there are four droplets inside the unit cell when the aggregate is in vibration and we will have to distinguish four sub-lattices to describe the vibration inside the two-dimensional aggregates. Calling  $(+,+)$  the state of a reference droplet, any droplet will have motions which can be represented by  $(+,+)$ ,  $(+,-)$ ,  $(-,+)$  or  $(-,-)$ , depending on its distance from the reference droplet.

We will first consider the case of square lattices for simplicity. In this case, because of the independence of the two principal directions ( $\mathbf{e}_1$  and  $\mathbf{e}_2$  are orthogonal), the two vibrations are not correlated. A droplet will oscillate independently along the two principal direction of the aggregate, at least at linear order. Figure 3(a) shows the

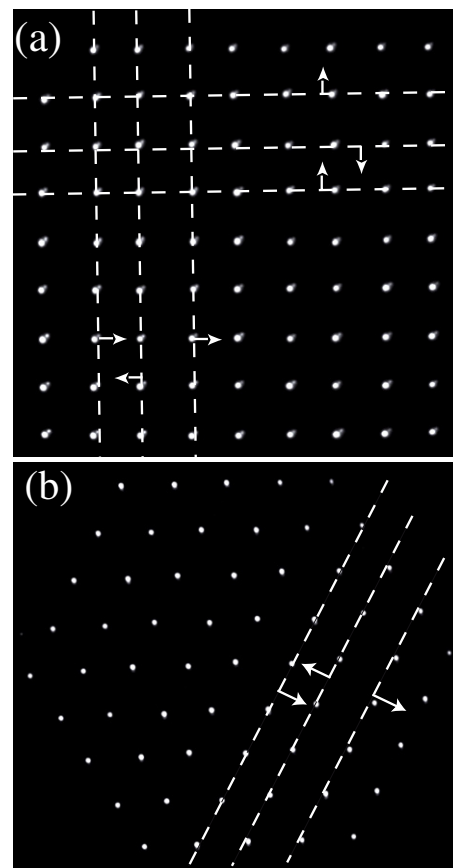


Fig. 4: (a) Snapshot showing the oscillations along the two possible direction of vibration in the square geometry. (b) Snapshot showing one of the possible oscillation modes in hexagonal geometry.

distribution of the different droplets in the aggregate. We obtain four sub-lattices having in-phase or counter-phase behaviours. For example, the motions of  $(+,+)$  and  $(+,-)$  droplets will be in phase along the  $\mathbf{e}_1$ -axis, but out of phase along the  $\mathbf{e}_2$ -axis. In *movie3.mov*, we can clearly distinguish these four sub-populations of droplets and verify their phase properties with respect to the other sub-lattices. The square geometry creates in-line vibration that are represented in fig. 4(a). The wavelength  $\lambda_V$  along each direction of the observed mode is the same as in the unidimensional case, with  $\lambda_V = 2L$ .

The case of hexagonal aggregates is more complex. Using the same principles as in the square case, we can define the state of any droplet by comparison with a reference droplet labeled  $(+,+)$ . The motion of any droplet can thus be represented by  $(+,+)$ ,  $(+,-)$ ,  $(-,+)$  or  $(-,-)$ , depending on its distance from the reference droplet (see fig. 3(b)). We also notice that there is one droplet of each sub-population inside the elementary cell. Nevertheless, because of the existence of a third symmetry axis, the vibrations along the  $\mathbf{e}_1$  and  $\mathbf{e}_2$  axes are coupled at linear order. This geometrical constraint implies a selection between the modes. Figure 4(b) presents one of

the possible modes, the same as that observed with liquid columns in two dimensions [15]). In this case, the selected mode has a wavelength  $\lambda_V = \sqrt{3}L$ .

**Phenomenological model.** – A theoretical description of these experimental observations should be able to describe the breaking of symmetry and the periodicity of the droplet lattice. What are the properties of the interaction between droplets? Each time a droplet bounces on the surface, it emits a surface wave. The superposition of these waves creates a periodic pattern on the surface. When a droplet falls on a distorted surface, it feels its local slope  $\alpha$  and receives an impulsion with a horizontal component. The equilibrium positions are thus located at the antinodes of the wave pattern. Displaced from its equilibrium position, the droplet tends to return to it. The applied force during a collision is proportional to the local slope  $\alpha$ .  $\alpha$  depends on the amplitude of the wave  $A_w$  as  $\alpha \sim A_w/\lambda_F$ . By changing  $\gamma_m$  we induce a variation of the amplitude  $A_w$  and thus a change in the shape of the potential trap for the droplet. In a mass-spring model, the spring constant associated with this potential will depend on the forcing acceleration.

We also need to take into account propagation effects. Each droplet feels the waves emitted by its neighbours at previous bounces: the waves need a time

$$\tau = \frac{L}{v_\varphi} \quad (2)$$

to propagate from their source to the next droplet. Assuming that the droplets are uniquely bound to their first neighbours, we can write a mass-spring chain model with these features.

For simplicity, we will consider only the one-dimensional case. Calling  $x_n$  the displacement of the  $n$ -th droplet from its equilibrium position, and  $m$  the mass of one droplet, we can write an equation of motion for the  $n$ -th droplet:

$$m \frac{d^2 x_n}{dt^2} = -\mu \frac{dx_n}{dt} + \tilde{A}f[x_n(t) - x_{n-1}(t-\tau)] + \tilde{A}f[x_{n+1}(t-\tau) - x_n(t)] \quad (3)$$

with  $\mu$  a damping coefficient,  $\tilde{A}$  the amplitude of the wave and  $f$  the interaction force between two neighbours, depending only on the positions of the droplets. The damping coefficient  $\mu$  stands for viscous effects, but also for the radiation losses of the  $n$ -th droplet. We can linearize this expression for small displacements, assuming that the interaction is proportional to the distance between the droplets. Equation (3) simplifies to

$$m \frac{d^2 x_n}{dt^2} = -\mu \frac{dx_n}{dt} + A[x_{n-1}(t-\tau) - 2x_n(t) + x_{n+1}(t-\tau)]. \quad (4)$$

As  $\tau \sim 1/f_F = 40$  ms is very small compared to the period of vibration of the pattern  $1/f_V \sim 1$  s, we can expand the interaction term. We thus assume, in agreement with

experimental observations, that the motion is slow with respect to the bouncing at  $f_F$ . We can write:

$$x_n(t-\tau) \simeq x_n(t) - \tau \frac{dx_n}{dt}. \quad (5)$$

Thus, we have

$$m \frac{d^2 x_n}{dt^2} = -\mu \frac{dx_n}{dt} - A\tau \left( \frac{dx_{n+1}}{dt} + \frac{dx_{n-1}}{dt} \right) + A(x_{n-1} - 2x_n + x_{n+1}). \quad (6)$$

We can now perform a linear stability analysis. We inject in this amplitude equation solutions with temporal and spatial periodicities  $x_n = X e^{i\omega_V t} e^{in\theta}$ ,  $\theta$  corresponding to a spatial phase, and we look for the instability threshold. This leads to

$$m\omega_V^2 = 4A \sin^2(\theta/2), \quad (7)$$

$$\mu + 2A\tau \cos \theta = 0. \quad (8)$$

Minimizing  $A$  with respect to  $\theta$  in order to get the most unstable mode, we get  $\cos \theta = -1$  which corresponds to  $\theta = \pi$ . Its wave number  $k_V = \frac{\pi}{L}$  is such that two successive droplets have opposite-phase motions. Equation (8) states that the instability threshold depends on the propagation time  $\tau$  between a droplet and its neighbours. If a droplet moves, its neighbours will feel it after a time delay  $\tau$  due to the finite velocity of the waves. This delay, provides irreversibility to the system and thus the time-symmetry breaking necessary for the growth of the instability. The threshold is  $A = \mu/(2\tau)$ , which, substituted into eq. (7) yields

$$f_V \propto \sqrt{\frac{1}{\tau}} \propto \sqrt{\frac{1}{L}}. \quad (9)$$

This theoretical prediction is in agreement with the experimental observations: the distance  $L$  between the droplets is not the same in the square or hexagonal geometries  $L = 8.1$  mm and  $L = 11.5$  mm, respectively, and the selected oscillation frequency  $f_V$  ( $f_V = 1.33$  Hz and  $f_V = 1$  Hz, respectively) decreases accordingly when  $L$  is increased.

**Finite-size effects.** – We have seen (see fig. 2) that the vibration amplitude is always smallest near the edges. We now investigate finite size effects by varying the length of the aggregate. We define  $\varepsilon = 1 - 2|\frac{n}{N+1} - \frac{1}{2}|$  the non-dimensional distance of the  $n$ -th droplet to the edge in an aggregate which is  $N$  droplets long and  $X_M$  the maximal amplitude in the aggregate. For aggregates (with square or hexagonal geometry) of length  $2 < N < 10$ , we look at the normalized amplitude  $X_n/X_M$  as a function of  $\varepsilon$  (see fig. 5). The amplitude is always largest at the center and decreases continuously getting closer to the edge.

This effect can be included in the model using the fact that a droplet located at the edge interacts with a single neighbour. Adding this condition in the equations is

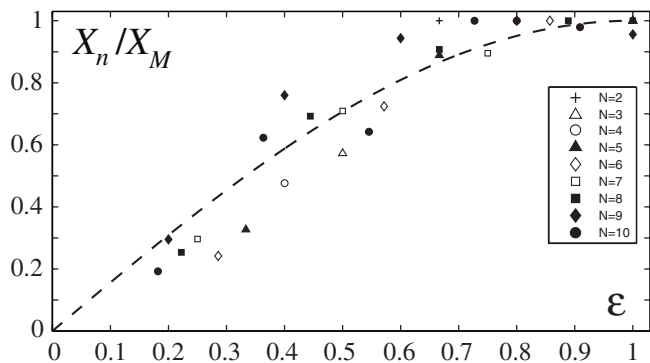


Fig. 5: Variation of the normalized amplitude of vibration  $X_n/X_M$  as a function of the non-dimensional distance to the edge  $\varepsilon$  for aggregates with length  $2 < N < 10$ . The dashed line corresponds to the theoretical prediction.

equivalent to write that, for a  $N$ -droplets-long aggregate, there exist two supplementary droplets (indexed by 0 and  $N+1$ ) that are at rest outside the aggregate. We deduce from the previous model that the amplitude of the motion of the  $n$ -th droplet is proportional to  $\sin(\varepsilon\pi/2)$ . The resulting curve, added to fig. 5 matches the experimental data for the hexagonal and the square lattices. For aggregates with  $N > 10$ , the agreement with this theoretical prediction becomes poorer, because of saturation effects at the center of the aggregate due to non-linear terms.

**Discussion.** – Is it possible to extend this model to two-dimensional aggregates? For square ones, the equations of vibration along the two principal directions appear to be independent because  $\mathbf{e}_1$  and  $\mathbf{e}_2$  are orthogonal. The apparent phase selection between the two vibrations should be interpreted by adding a non-linear coupling in the amplitude equations. In the hexagonal geometry, the existence of a third symmetry axis implies a selection of the vibration mode at linear order. A complete study of the allowed two-dimensional modes in the hexagonal symmetry has been performed by Pirat *et al.* [16], pointing out the existence of only 20 different possibilities. In the experiments reported here, we always observe a combination of some of them. A complete analysis of the two-dimensional case should take into account not only the coupling between the principal directions, but also the existence of edges. This study is beyond the scope of this experimental article, and should be reserved for a further communication.

The coherent vibration inside regular droplet aggregates is reminiscent of phonons in crystalline lattices. Here, we have a mass-spring chain oscillating with a coherent mode, but only a single value in the vibration spectrum is excited. This is different from the phonon excitation in crystalline lattices by temperature: in that case, the whole spectrum is excited and vibrational energy is distributed according to the energy of each mode. In our experiment,

the observed mode is that with the highest energy. This mode selection is related to the nature of the excitation. The motion of each droplet is induced by the surface waves emitted by its neighbours at previous bounces. The propagation time between the droplets provides irreversibility in the system and thus the time-symmetry breaking needed for the growth of the instability. The system then selects a single wavelength along a line of droplets.

The melting of the aggregates occurring from the center, contrary to the classical melting process occurring at the edges, is a consequence of this specific selection process. The oscillations are not due to a thermal excitation distributed randomly all over the aggregate, but from a coherent excitation by the surface waves. As the wave amplitude is maximal at the center, the central droplets are the first which are able to leave their potential trap leading to a core destruction of the aggregate

\*\*\*

We are grateful to G. COUPIER, E. FORT, A. GRADOS, J. MOUKHTAR, G. PUCCI, M. RECEVEUR and L. RHÉA. This work has been supported by the ANR 06-BLAN-0297-03.

## REFERENCES

- [1] COUDER Y., FORT E., GAUTIER C. H. and BOUDAUD A., *Phys. Rev. Lett.*, **94** (2005) 177801.
- [2] PROTIERE S., BOUDAUD A. and COUDER Y., *J. Fluid Mech.*, **554** (2006) 85.
- [3] EDDI A., TERWAGNE D., FORT E. and COUDER Y., *EPL*, **82** (2008) 44001.
- [4] LIEBER S. I., HERDERSHOTT M. C., PATTANAPORKRATAN A. and MACLENNAN J. E., *Phys. Rev. E*, **75** (2007) 056308.
- [5] VANDEWALLE N., TERWAGNE D., MULLENERS K., GILET T. and DORBOLO S., *Phys. Fluids*, **18** (2006) 091106.
- [6] FARADAY M., *Philos. Trans. R. Soc. London*, **52** (1831) 299.
- [7] DOUADY S. and FAUVE S., *Europhys. Lett.*, **6** (1988) 221.
- [8] EDDI A., DECELLE A., FORT E. and COUDER Y., *EPL*, **87** (2009) 56002.
- [9] COULET P. and IOOSS G., *Phys. Rev. Lett.*, **64** (1990) 866.
- [10] ANDERECK A., LIU S. S. and SWINNEY H. L., *J. Fluid Mech.*, **174** (1986) 155.
- [11] DUBOIS M., BERGE P., DA SILVA R., DAVIAUD F. and PETROV A., *Europhys. Lett.*, **8** (1989) 135.
- [12] RABAUD M., MICHALLAND S. and COUDER Y., *Phys. Rev. Lett.*, **64** (1990) 184.
- [13] BRUNET P., FLESSELLES J. M. and LIMAT L., *Eur. Phys. J. B*, **35** (525) 2003.
- [14] GINIBRE M., AKAMATSU S. and FAIVRE G., *Phys. Rev. E*, **56** (1997) 780.
- [15] PIRAT C., MATHIS C., MAÏSSA P. and GIL L., *Phys. Rev. Lett.*, **92** (2004) 104501.
- [16] PIRAT C. and GIL L., *Physica D*, **179** (2003) 92.